Journal of Materials Chemistry C

ROYAL SOCIETY OF CHEMISTRY

PAPER

View Article Online
View Journal | View Issue

Check for updates

Cite this: J. Mater. Chem. C, 2023, 11, 16066

Synthesis of barium hexaferrite nano-platelets for ethylene glycol ferrofluids

Y. Ahmed,[a] A. Paul,[b] P. Hribar Boštjančič,[c] A. Mertelj,[c] D. Lisjak[d] and D. Zabek*[a]

Received 20th October 2023,
Accepted 3rd November 2023

DOI: 10.1039/d3tc03833e

rsc.li/materials-c

Recently discovered barium hexaferrite ($BaFe_{12}O_{19}$)-based nanoplatelets form a ferromagnetic–ferrofluid which exhibits interesting magnetic properties. Manufacturing the barium hexaferrite nano-platelets *via* hydrothermal synthesis remains of fundamental interest and allows for optimisation of structural, magnetic, and morphological properties, which impact on ferrofluid properties. This report describes a surfactant assisted manufacturing method for an ethylene glycol based ferrofluid using hexadecyltrimethylammonium bromide (CTAB) with barium hexaferrite nano-platelets. A hexagonal nano-platelet morphology with a typical diameter up to 200 nm and thickness of a few nanometres was observed by transmission electron microscopy (TEM) with stable concentrations between 10–200 mg ml^{-1}, while saturation magnetisation of dry particles was measured at 32.8 A m^2 kg^{-1} using a vibrating sample magnetometer (VSM). The manufactured barium hexaferrite–ethylene glycol ferrofluid exhibits improved thermal properties compared to previously used butanol based ferrofluids, opening the way into new applications in the field of colloidal suspensions.

1. Introduction

Ferrofluids are stable colloidal dispersions of magnetic particles suspended in a carrier fluid exhibiting rheological and magnetic properties. The rheological properties of a ferrofluid largely depend on the Brownian motion of the suspended particles as well as the particle shape and intrinsic magnetic properties.[1] Most ferrofluids are based on iron oxide – Fe_3O_4 nanoparticles with a spherical shape and an approximate diameter of 10–20 nm *i.e.*, superparamagnetic nanoparticles.[2] These fluids have a wide range of commercial applications covering industrial coolants, sealants, light switching, hyperthermia, defect sensors, and drug targeting.[3] On the other hand, non-spherical magnetic nanoparticles exhibit a high level of shape anisotropy with distinct magnetic properties.[4] Non-spherical particles are of great interest because of the correlation between their magnetic properties, size, and shape. In particular, non-spherical magnetic particles such as nanorods and nanoplatelets display significantly different rheological properties compared to spherical particles. Nanoplatelets, or thin disks, are of fundamental interest due to their high aspect ratio and anisotropic magnetic properties, examples of which include hexaferrites, Co nano-discs[5,6] and Fe_3O_4 nanoplates on graphene films.[7] Hexagonal ferrites/hexaferrites have become increasingly sought after since their discovery in the 1950s due to their high magnetic coercivity with the most known ferrites containing Ba or Sr as divalent cations. Barium hexaferrites – $BaFe_{12}O_{19}$ (BHF) exhibit a hexagonal shape shown by Went *et al.* and their diameter depends on the synthesis method used. The highly anisotropic crystal structure of BHF produces its magnetocrystalline anisotropy and allows for BHF and its derivatives to be used for permanent magnets, magnetic-recording media and microwave applications.[8] Barium hexaferrites exhibits a high uniaxial magnetocrystalline anisotropy (K_i = 3.3 × 10^4 J m^{-3}) with the magnetic easy axis parallel to the crystallographic *c*-axis, producing a high coercivity.[9] Their magnetic anisotropy allows hexaferrites to be used at much higher frequencies compared to spinel ferrites or garnets,[10] and applications above 30 GHz. BHF nanoparticles have also received increased attention for a range of applications due to their easy axis oriented along the *c*-direction, *i.e.*, perpendicular to the nanoplatelet basal surface.[11,12] This makes them good candidates for non-thermic magneto-mechanical cancer treatment where the mechanical rotation of the nanoparticles creates a shear in an alternating magnetic field which can be used to damage cancer cells.[13] Barium hexaferrites also create a nematic order in a ferrofluid which exhibits macroscopic magnetic and optical effects forming ferromagnetic–ferrofluids with macroscopic permanent magnet properties in a fluid.[14]

[a] School of Engineering, Cardiff University, CF24 3AA, Cardiff, UK. E-mail: Zabekd@cardiff.ac.uk
[b] School of Chemistry, Cardiff University, CF10 3AT, Cardiff, UK
[c] Department of Complex Matter, Jozef Stefan Institute, SI-1000 Ljubljana, Slovenia
[d] Department of Material Synthesis, Jozef Stefan Institute, SI-1000 Ljubljana, Slovenia

Several synthesis methods to manufacture BHF nanoparticles exist, including coprecipitation[10] and hydrothermal synthesis.[15] Hydrothermal synthesis is advantageous over coprecipitation methods due to direct synthesis of the nanoparticles without the need for additional high-temperature reaction in solid-state, allowing for easy dispersion. Several advancements on the hydrothermal synthesis of BHF have helped to understand the synthesis mechanism and key parameters which optimise their growth. Low temperature hydrothermal synthesis below 150 °C produces superparamagnetic BHF nanoparticles[16] which have a considerable advantage of easy dispersion in a variety of liquids, however, their poor room temperature magnetizations below 10 A m^2 kg^{-1} (at 5 T) prompts the need for larger particles exhibiting higher levels of magnetisation. Temperatures of up to 240 °C are required for the synthesis of magnetically applicable particles for which secondary recrystallisation, or the Ostwald ripening effect, is prevented through doping.[14] For the high temperature hydrothermal synthesis of BHF nanoparticles, the partial substitution of Fe^{3+} ions with Sc^{3+} allows for a much greater control on the size distribution of nanoparticles. The partial substitution of Sc^{3+} into the BHF structure also increases magnetic saturation which is an opposite effect to that in the bulk.[17] Another synthesis method to control particle shape and size is to use surfactants. Oleic acid adsorbed onto the nanoparticle surface acts as surfactant and can be used to block the secondary recrystallisation of BHF nanoparticles at high temperature synthesis, however, the growth of the nanoparticles was completely blocked producing superparamagnetic nanoparticles.[18] Subsequently, adsorption of organic molecules to the surface of BHF nanoparticles has been explored to aid colloidal stability of the nanoparticles that display permanent magnetic moments resulting in the long-range magnetic dipole–dipole interactions between each particle.[19] Repulsive forces in the form of electrostatic, steric, or a combination of both, must be introduced to counteract these attractive interactions and consequently achieve colloidal stability in aqueous media.[20] In previous studies the surface of BHF nanoparticles has been modified by various methods such as electrostatic adsorption of charged surfactants, ligands, or polymer brushes,[21] coating of a continuous polymer film,[22] direct grafting of surfactants or polymers, and attachment of biological molecules.[23] Other methods of attaching stabilizing polymer, such as *e.g.* dextran, to BHF surfaces have also been explored for dispersion in complex biological media and paved the way towards some biomedical applications.[19] A highly stable dispersion of BHF nanoparticles is possible in 1-butanol *via* electrosteric stabilization through dodecylbenzenesulfonic acid (DBSA) surface attachment.[24] Electrostatic repulsion is due to the dissociation of the sulfonic group in water while steric repulsion is a direct result of the long carbon chain of the DBSA surfactant.

In this report we describe a surfactant assisted manufacturing method for an ethylene glycol based ferrofluid using hexadecyltrimethylammonium bromide (CTAB) with BHF nano-platelets followed by a complete magnetic, microscopic, and electrostatic characterisation. The proposed ethylene glycol based ferromagnetic–ferrofluid exhibits great stability and low volatility with excellent thermal properties, and therefore opens the way for commercial applications.

2. Experimental

Barium hexaferrite – BHF ($BaFe_{12}O_{19}$) nano-platelets were manufactured *via* hydrothermal synthesis. Barium nitrate (99%), nitric acid (70%) and ethylene glycol (99%) were obtained from Thermo-Fisher scientific. 1-Butanol (99%), scandium(III) nitrate hydrate (99%) and iron(III) nitrate nonhydrate (98%) were obtained from Alfa-Aesar. Sodium hydroxide (98%), DBSA (95%) and CTAB (98%) were obtained from Sigma-Aldrich.

Synthesis and preparation of the ferrofluids

Sc-substituted BHF nanoparticles were hydrothermally synthesised at 190 °C following a previously reported procedure.[17] The BHF nanoparticles were functionalised with either DBSA or CTAB. For the preparation of BHF nanoparticles, the barium, iron(III) and scandium(III) nitrates were dissolved in deionized water in a molar ratio of 1 : 4.5 : 0.5. An excess of sodium hydroxide was gradually added after which precipitation occurs and the solution was allowed to cool to room temperature. After precipitation, a solution of DBSA (in 25 ml of acetone), or CTAB (in 25 ml of water), was gradually added to the reaction mixture. To produce DBSA-coated BHF nanoparticles, this mixture is allowed to stir for an additional 30 minutes whereas for CTAB-coated BHF nanoparticles, the mixture was stirred overnight. The autoclave was heated to 190 °C at a heating rate of 3 °C min^{-1} after which it was allowed to cool to 20 °C at 3 °C min^{-1}. We facilitated identical growth conditions for both surfactants while maintaining a low synthesis temperature to prevent surfactant degradation. Subsequently, we were able to confirm that a synthesis temperature of above 150 °C is required to produce magnetically applicable BHF nanoparticles.[25] The resultant nanoparticles were centrifuged at 201 rcf for 5 min and washed with water. The nanoparticles were dispersed in 60 ml of water and the pH was adjusted to 1.5 for DBSA coated BHF nanoparticles and 4.6 for CTAB coated BHF nanoparticles using nitric acid. The mixture was heated to 100 °C for 2 h on stirring. The nanoparticles were centrifuged, the DBSA coated nanoparticles were washed with water and acetone while the CTAB coated nanoparticles are only washed with water. The DBSA coated nanoparticles were dried at 60 °C and subsequently dispersed in 1-butanol to create a ferrofluid which is herein referred to as DBSA/BHF. CTAB coated nanoparticles were dispersed in ethylene glycol without prior drying to create a ferrofluid referred to as CTAB/BHF in this report. Ultrasonication (Fisherbrand) at 35 W for 2 hours was used to disperse the surfactant coated nanoparticles and make up a concentration of 100 mg ml^{-1} DBSA/BHF and CTAB/BHF ferrofluid.

Characterisation of materials

Fig. 1 shows the transmission electrom microscopy – TEM scans (TEM, Jeol2100) of the (a) CTAB dried from ethylenegylcol and (b) DBSA dried form 1-butanol BHF samples. A drop of the

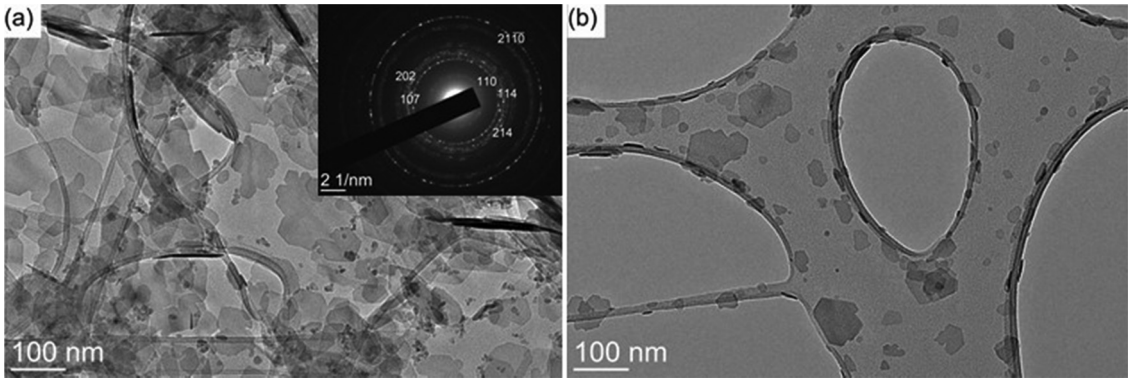

Fig. 1 TEM images of the nanoplatelets coated with: (a) CTAB dried from ethylenegylcol and (b) DBSA dried form 1-butanol. Insertion in panel (a) shows SAED with indices corresponding the barium hexaferrite structure, space group $P6_3/mmc$ (194).

diluted suspension was deposited on a Cu-coated TEM supporting grid and left to dry. Most of the nanoplatelets lie flat on the TEM grid showing a broad distribution. The BHF particle size is defined as the maximum, or equivalent, diameter of a hexagonal particle in this report and the size distribution was determined using DigitalMicrograph® software. More than 500 particles were counted for statistics. The CTAB-coated BHF nanopletelets dispersed in EG had very broad distribution of their diameters (Fig. 1). The largest CTAB-coated BHF nanoplatelets had diameters of few hundreds of nanometres while the smallest discoids had diameters of 10 nm or less. The hexaferrite structure and ferrimagnetic order is confirmed by the selected area electron diffraction – SAED inset in Fig. 1(a) with indices corresponding to barium hexaferrite structure space group $P6_3/mmc$ (194) for particles greater than 10 nm diameter while smaller particles do not evolve in the discoids.[26]

Fig. 2 shows the particle size distribution of the BHF nanoparticles DBSA/BHF and CTAB/BHF. The size distribution of DBSA coated nanoparticles shows particle diameters of up to 100 nm compared to CTAB coated nanoparticles with diameters of up to 180 nm. Samples with a broader size range were found to sediment in solvent much faster than samples with a narrow size distribution despite the electrostatic repulsion provided by the surfactant. Subsequently, it has also been observed that nanoparticles with diameters of a few hundred nanometers aggregate before sedimenting.[20] The DBSA-coated nanoplatelets dispersed in 1-butanol also had a thickness of few nanometres but smaller diameters than the CTAB-coated nanoplatelets. The resulting mean diameter was 32 nm with a standard deviation of 26 nm for DBSA/BHF while CTAB/BHF had a mean diameter of 26 nm with a standard deviation of 52 nm.

The synthesised DBSA and CTAB-coated BHF nanoparticles were magnetically analysed using vibrating-sample magnetometer – VSM (LakeShore 7400). The VSM samples were prepared into 3 mm wide tablets with an applied mechanical force of approximately 1000 N mm^{-2} for 5 seconds. Fig. 3 shows a distinct magnetic hysteresis loop at excitation fields between −1000 kA m^{-1} and +1000 kA m^{-1} for the DBSA/BHF and CTAB/BHF dry particles which is typical of a hard ferrimagnetic

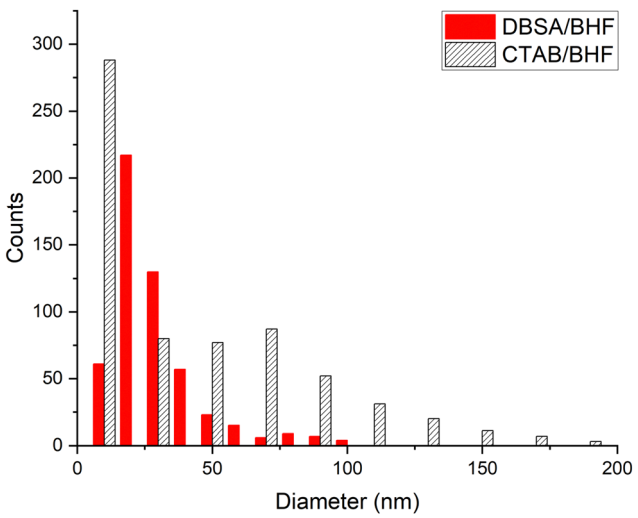

Fig. 2 Diameter distribution of the nanoplatelets produced at 190 °C: CTAB/BHF dispersed in ethylene glycol and DBSA/BHF dispersed in 1-butanol.

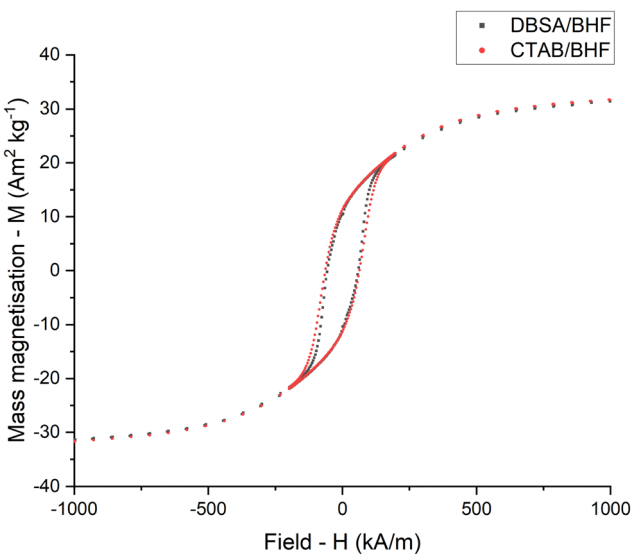

Fig. 3 Mass magnetisation – M against applied field – H of barium hexaferrite nanoparticles coated with DBSA and CTAB.

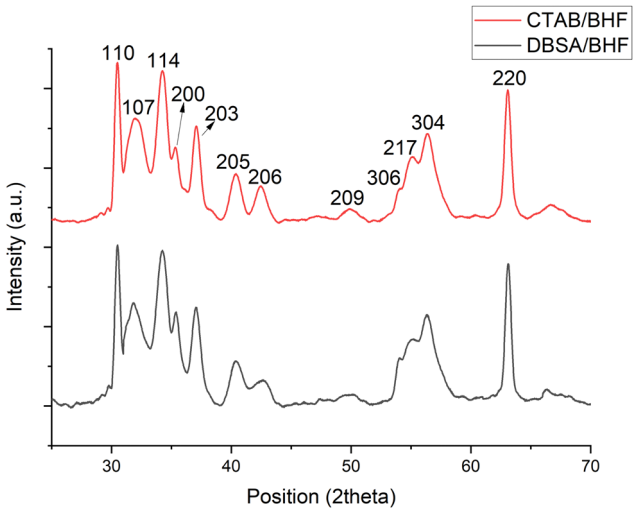

Fig. 4 XRD patterns of DBSA/BHF and CTAB/BHF coated barium hexaferrite with labelled crystallographic planes corresponding to hexagonally crystal symmetry (space group $P6_3/mmc$) BHF nanoparticles.

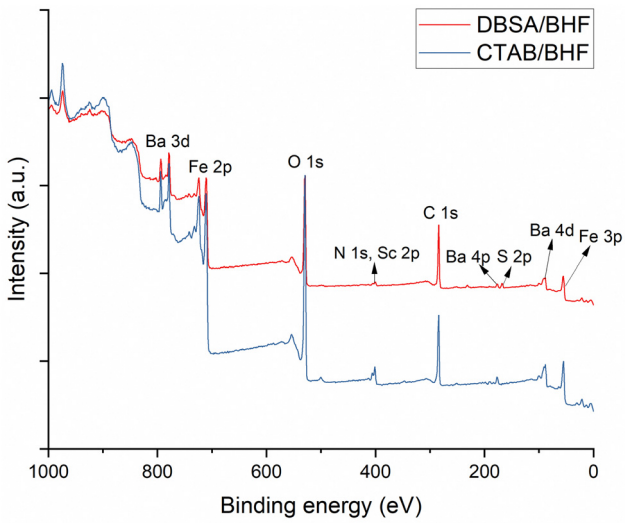

Fig. 5 XPS spectra of dry DBSA and CTAB coated BHF nanoparticles.

material. The pressed tablets exhibit specific magnetic remanence M_r = 10.4 A m^2 kg^{-1}, coercivity H_c = 72 [kA m^{-1}] and magnetic saturation M_s = 32.8 A m^2 kg^{-1}. The reported values correspond with previous findings for Sc-doped BHF nanoparticles for remancence, coercicity and saturation.[1] For comparison the crystallographic structure of dry DBSA and CTAB-coated BHF nanoparticles was analysed using X-Ray Diffraction – XRD (Panalytical Xpert Pro XRD). Fig. 4 shows the XRD diffraction patterns of DBSA and CTAB-coated BHF nanoparticles with labelled crystallographic planes. Both DBSA/BHF and CTAB/BHF show a similar diffraction pattern corresponding to hexagonally shaped BHF nanoparticles. BHF has the magnetoplumbite crystal structure and is highly anisotropic with a = 0.589 nm and c = 2.32 nm, because of which they have a preferred growth in the ab-plane with limited growth in the c-direction. The crystal structure is identified by the stacking sequence RSR*S* of the basic blocks S and R, where the asterisk denotes the rotation of the block by 180° around the hexagonal c-axis.[27] The Ba^{2+} ions within this sequence are located within the middle of the R block, while the Fe^{3+} ions occupy five different crystallographic sites within the R and S blocks. The ($hk0$) peaks (110) and (220) are relatively sharp which indicates the presence of large BHF nanoparticles, whereas the broad (hkl where $l \neq 0$) relate to the thickness of the nanoparticles.[18] The ($hk0$) peaks have a much larger intensity which agrees with the growth mechanism and TEM results in Fig. 1 showing the width of the nanoparticles being larger than the thickness (10 nm).

The functionalization of both DBSA and CTAB surfactant to the surface of BHF nanoparticles can be studied using X-ray photoelectron spectroscopy – XPS (Kratos Axis Ultra DLD) measurements on dry nanoparticles using monochromatic AI Kα X-ray source (photon energy 1486.6 eV) operating at 120 W (10 mA × 12 kV). All samples were pressed into recesses of a modified Kratos Axis Ultra standard sample bar and pressed flat with an iso-propyl alcohol cleaned glass slides before insertion into the spectrometer. Fig. 5 shows the XPS data for both DBSA/BHF and CTAB/BHF with characteristic peaks for Ba/3d (779 eV), Fe/2p (711 eV), O/1s (530 eV), Sc/2p (402 eV) (originating from the BHF nanoparticles) and C/1s (284 eV) which is considered a reference peak. For DBSA/BHF an extra peak for S/2p (168 eV) is observed and attributed to the sulfur head group of the DBSA surfactant, this peak is not observed in the XPS data for pure BHF nanoparticles or CTAB/BHF.[24,28] For CTAB/BHF, the C–NH_2 peak corresponding to the CTAB surfactant head group occurs at 400 eV near the Sc/2p peak. XPS data for pure BHF nanoparticles generally show a carbon concentration of approximately 24%, this also increases as the surfactants adsorb onto the particle surface to 46% for DBSA/BHF and 35% for CTAB/BHF (Fig. 6).

The thermal decomposition of DBSA/BHF and CTAB/BHF powder samples were analysed using thermogravimetric analysis – TGA

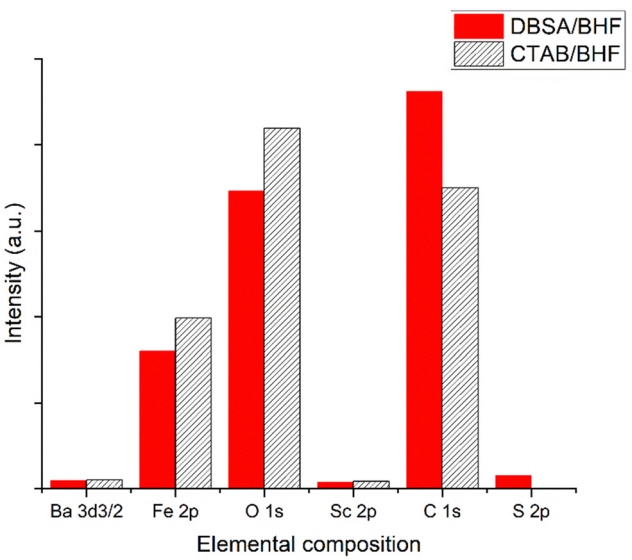

Fig. 6 Surface elemental composition of dry DBSA and CTAB coated BHF nanoparticle powders.

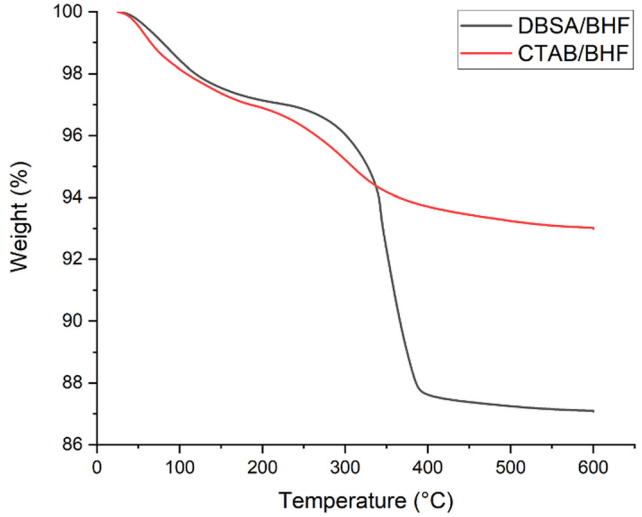

Fig. 7 Thermal decomposition (TGA) curves of DBSA/BHF and CTAB/BHF powder samples heated from 25 °C to 600 °C at 10 °C min^{-1} in air.

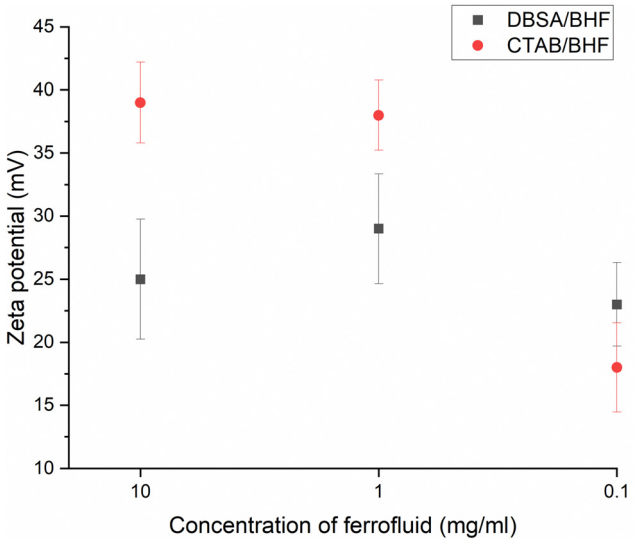

Fig. 8 Zeta potential data for the DBSA/BHF ferrofluid in butanol and CTAB/BHF in ethylene glycol with standard deviation for zeta potential-measurements.

(Mettler Toledo) shown in Fig. 7. The samples were heated from 25 °C to 600 °C at 10 °C min^{-1} under an inert atmosphere (air) with gas flow of 100 ml min^{-1}. According to Fig. 7, the mass fraction of surfactant molecules, *i.e.* the total molar concentration of surfactant molecules present around the particles (c-tot), is later used to calculate the amount of surfactant molecules adsorbed onto the nanoparticle surface once dispersed in solvent. We found DBSA surfactant to decompose at approximately 265 °C with a mass fraction of approximately 13% while CTAB decomposes at approximately 235 °C with a mass fraction of 7%.[19] According to Fig. 6, there is also a greater increase of surface carbon for DBSA/BHF which agrees with the TGA data showing a higher average adsorption of DBSA on the BHF surface than CTAB. The Ba/Fe atomic ratio (0.05) was lower than the stoichiometric value (0.13 in $BaFe_{12}O_{19}$) which suggests that the surface of nanoparticles is rich in Fe.[29]

3. Results and discussion

Colloidal stability is crucial for a ferrofluid because long reaching magnetic forces between individual particles quickly lead to aggregation and sedimentation. In order to compare the manufactured suspension stability, and therefore determine the quality of the ferrofluid, electrophoretic mobility and zeta potential measurements were obtained for both DBSA/BHF and CTAB/BHF products.[20] The zeta potential values of 1 mg ml^{-1} DBSA/BHF and CTAB/BHF suspensions in butanol and ethylene glycol respectively were measured on a Malvern Nano-Z zeta analyser using a disposable capillary folding cell at an applied electric field of 20 V mm^{-1}. Eqn (1) shows the Helmholtz–Smoluchowski equation used to calculate the zeta potential from electrophoretic mobility, where ζ (mV) is the zeta potential and μ_e (μm cm V^{-1} s^{-1}) is the electrophoretic mobility of the particles, η (mPa s) is the viscosity of the medium and $f(\kappa a)$ is the Debye function set to 1.5, as follows:

$$\zeta = \frac{4\pi\eta}{\varepsilon} f(\kappa a) \cdot \mu_e \quad (1)$$

100 mg ml^{-1} samples of DBSA/BHF in butanol and CTAB/BHF in ethylene glycol were diluted with pure solvent to make 10, 1 and 0.1 mg ml^{-1} nanoparticle weight to volume concentrations for zeta potential measurements to be conducted at 25 °C. According to Fig. 8, the zeta potential for DBSA/BHF was found to be 29.9 ± 4.4 mV and lower than the 38.3 ± 2.8 mV for CTAB/BHF ferrofluid using pure solvent permittivity and viscosity values from Table 1, which indicates a weaker electrostatic repulsion for DBSA coated BHF nanoparticles. The zeta potential values for both DBSA/BHF and CTAB/BHF suggest that the resulting ferrofluids are reasonably stable with the BHF nanoparticles fully dispersed in their respective carrier fluids.[30] The positive zeta potential values for both ferrofluids are due to a protonation of the surface groups at the particle–solvent interface. For the CTAB/BHF ferrofluid, the zeta potential stays constant from 1–10 mg ml^{-1} and significantly depletes at 0.1 mg ml^{-1} (Fig. 8). This depletion could be due to an over-dilution of the ferrofluid leading to a lack of surfactant molecules on the surface of the BHF nanoparticles. A similar zeta potential is observed at 0.1 mg ml^{-1} for DBSA/BHF ferrofluid while there is an expectedly low zeta potential observed at 10 mg ml^{-1} with the highest value measured at 1 mg ml^{-1}.

The surface modification of the BHF nanoparticles with a layer of surfactant allows for the formation of a stable colloidal suspension. The surfactant molecules are adsorbed onto the nanoparticle surface which is created through dissociation of the surfactant head group counterion in water during the synthesis stage. To determine the quantity of the CTAB surfactant adsorbed onto the BHF nanoparticle surface and the amount dissolved in the ethylene glycol liquid carrier, the molar concentration of dissolved CTAB surfactant (c-dis) was determined through electrical conductivity σ (μS cm^{-1}) measurements (Mettler Toledo, LE703). The conductivity of CTAB/BHF in ethylene glycol and DBSA/BHF in butanol was measured at 10 and 100 mg ml^{-1} at room temperature. The amount of dissolved

Table 1 Electrophoretic mobility and zeta potential of the DBSA/BHF in butanol and CTAB/BHF in ethylene glycol

Ferrofluid	Relative permittivity of the solvent ε_r [−]	Viscosity η of the solvent (mPa s)	Conductivity (μS cm^{-1})	μ_e (μm cm V^{-1} s^{-1})	ζ (mV)
DBSA/BHF	17.6	2.6	0.00108 ± 0.001%	0.221	29.9 ± 4.4
CTAB/BHF	37.0	16.2	0.00252 ± 0.001%	0.080	38.3 ± 2.8

Table 2 Concentrations of the dissolved (c-dis) and adsorbed (c-ads) DBSA/BHF in 1-butanol and CTAB/BHF in ethylene glycol suspensions at 10 and 100 mg ml^{-1}

Ferrofluid concentration (mg ml^{-1})	c-dis (mM)		c-ads (mM)		c-ads/c-tot	
	DBSA/BHF	CTAB/BHF	DBSA/BHF	CTAB/BHF	DBSA/BHF	CTAB/BHF
10	2.5	0.37	1.21	1.99	0.32	0.85
100	6.1	3.57	26.2	19.6	0.81	0.85

CTAB c-dis was determined through an addition method by gradually adding equal amounts of powder CTAB surfactant into the suspension while continuously stirring the solution. The conductivity was measured after each addition of surfactant and found to linearly increase with the increase of c-dis. The linear equation $\sigma = a + (b \times (\Delta\text{c-dis}))$ was used to calculate c-dis as a quotient of '*a*' and '*b*' (Table 2). The amount of CTAB surfactant adsorbed (c-ads) on the surface of the BHF nanoparticles was calculated from the difference between the total molar concentration of CTAB (c-tot) and c-dis. The mass fraction of CTAB in a known sample mass of dry BHF nanoparticles was determined by TGA for adsorbed surfactant calculations. Conductivity measurements (Table 2) for CTAB/BHF ferrofluid show that c-ads is unaffected by concentration and the ratio of c-ads/c-tot remains 0.85 for 10 and 100 mg ml^{-1}. This is consistent with the zeta potential for CTAB/BHF ferrofluid being constant for 1–10 mg ml^{-1}, as the amount of CTAB surfactant on the BHF nanoparticle surface remains the same. On the other hand, c-ads varies between concentrations for DBSA/BHF ferrofluid as the ratio of c-ads/c-tot at 100 mg ml^{-1} was comparable with CTAB/BHF but significantly lower at 10 mg ml^{-1}. This indicates that the CTAB surfactant is more strongly bonded to the BHF nanoparticle surface than DBSA as the dilution of ferrofluid does not increase c-dis. However, visual observations of both DBSA/BHF and CTAB/BHF ferrofluids remain stable between 10–100 mg ml^{-1} indicating other factors such as dielectric constant of solvent, particle size distribution, and an equilibrium between c-dis and c-ads ensure stability of ferrofluid.

Fig. 9 shows a simple visual experiment to compare the stability of both CTAB/BHF and DBSA/BHF ferrofluids which was conducted by exposing the ferrofluids to a strong permanent external magnetic field and inspecting the time it takes to separate magnetic nanoparticles from the liquid carrier. The experiment was carried out by placing a permanent magnet (permanent external magnetic field = 0.3 T) against the side of each vial filled with the synthesised ferrofluid which attracts most of the ferrofluid creating a vertical sloped gradient perpendicular to gravity acting downwards. A concentration of 40 mg ml^{-1} was selected where the magnetic energy is equal to the gravitational energy creating a gradual slope. This slope shortens overtime while the volume of the carrier fluid rises at the bottom of the vial as the BHF nanoparticles precipitate out of the medium. For an identical volume of 1 ml and concentration of 40 mg ml^{-1} for DBSA/BHF–butanol and CTAB/BHF–ethylene glycol ferrofluid, the height of the carrier fluid remaining at the bottom of the vial after 1, 10, 100, and 1000 minutes were determined from photographs, and taken as a relative indicator of destabilization over time when exposed to an external magnetic field. Although both ferrofluids show destabilization at each increment measured, it can be argued that despite difference in carrier fluid viscosity the DBSA/BHF ferrofluid is more stable as it showed a smaller rise in carrier fluid column from 1–100 minutes, compared to CTAB/BHF. Overall, both DBSA/BHF and CTAB/BHF showed a gradual destabilization from 1–100 minutes meaning that the BHF nanoparticles retained some degree of dispersion within their carrier fluids. After 1000 minutes, both ferrofluids were mostly destabilized only showing a shallow gradient compared to the

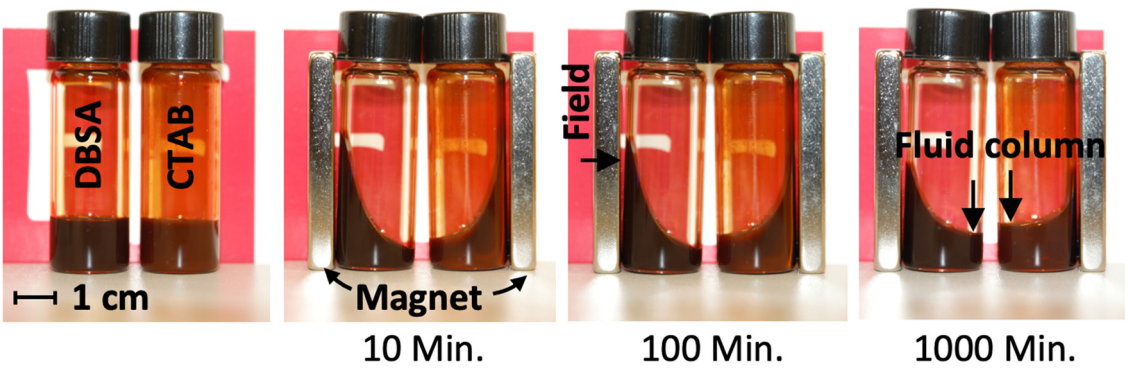

Fig. 9 Experimental destabilization times of DBSA/BHF and CTAB/BHF ferrofluid (40 mg ml^{-1}) exposed to a permanent magnetic field (0.3 T).

image taken after 10 minutes but can be redispersed by sonication. The here produced CTAB/BHF ferrofluid in ethylene glycol has a boiling temperature of 197.35 °C exhibiting superior thermal properties compared to DBSA/BHF ferrofluid in butanol with a boiling temperature of 117.45 °C.[31] Since ethylene glycol is commonly used as a plasticizing agent, automotive antifreeze, and other heat transfer applications the proposed ferrofluid can be explored in various real world engineering applications. Finally, ethylene glycol also has a low vapour pressure and low volumetric expansion coefficient potentially, opening the way into new ferrofluid applications.

4. Conclusions

We developed a new barium hexaferrite (BHF) based ferrofluid and stabilised the ferrofluid using hexadecyltrimethylammonium bromide (CTAB) surfactant through electrostatic and steric repulsion. Dry hexadecyltrimethylammonium bromide coated barium hexaferrite nanoparticles with an average size up to 200 nm were characterised using powder X-ray diffraction (XRD), transmission electron microscopy (TEM), thermogravimetric analysis (TGA), and vibrating-sample magnetometer (VSM) techniques. Surface properties of the nanoparticles were analysed through X-ray photoelectron spectroscopy (XPS). Despite differences in size distribution and surface properties, the synthesised nanoparticles exhibit identical magnetic properties compared to previously reported dodecyl benzene sulphonic acid (DBSA) coated nanoparticles. Subsequently, the surfactant coated barium hexaferrite nanoparticles were dispersed in ethylene glycol to create a ferrofluid and the colloidal stability was measured using zeta potential and compared with that of a butanol ferrofluid at different concentrations. Zeta potential for hexadecyltrimethylammonium bromide coated nanoparticles was consistently higher than dodecylbenzenesulfonic acid coated barium hexaferrite nanoparticles at the same concentration. Through conductivity measurements, hexadecyltrimethylammonium bromide was found to be more strongly bonded to the nanoparticle surface than dodecylbenzenesulfonic acid as the amount of surfactant adsorbed stays consistent despite dilution of the ferrofluid. Colloidal stability is best observed in the laboratory through identifying signs of sedimentation and flocculation of nanoparticles with and without the presence of an external magnetic field. Both hexadecyltrimethylammonium bromide and dodecylbenzenesulfonic acid coated barium hexaferrite nanoparticles produce ferrofluids that are stable for a sufficiently long period of time. The applicability of both ferrofluids can be compared with regards to their carrier fluid, as the proposed ethylene glycol solvent exhibits superior properties compared to the previously reported butanol because of its higher boiling point and miscibility in water, whereas butanol is an extremely volatile solvent and has limited miscibility in water. This ensures the potential for a variety of applications for barium hexaferrite ferrofluids stabilized with hexadecyltrimethylammonium bromide as opposed to dodecylbenzenesulfonic acid surfactant because of its stable dispersion in ethylene glycol. Since the exchange of carrier fluids also has rheological implications, future work also includes rheological measurements for ethylene glycol based BHF ferrofluids.

Conflicts of interest

There are no conflicts to declare.

Acknowledgements

This research received funding from the Royal Academy of Engineering (RAEng) under the Research Fellowship Program Number RF\201819\18\202, and Slovenian Research and Innovation Agency under grants P1-0192 and P2-0089.

References

1 D. Lisjak and A. Mertelj, Anisotropic Magnetic Nanoparticles: A Review of Their Properties, Syntheses and Potential Applications, *Prog. Mater. Sci.*, 2018, **95**, 286–328, DOI: **10.1016/j.pmatsci.2018.03.003**.

2 L. Maldonado-Camargo, M. Unni and C. Rinaldi, Magnetic Characterization of Iron Oxide Nanoparticles for Biomedical Applications, in *Biomedical Nanotechnology*, ed. S. H. Petrosko and E. S. Day, Methods in Molecular Biology, Springer, New York, New York, NY, 2017, vol. 1570, pp. 47–71, DOI: **10.1007/978-1-4939-6840-4_4**.

3 J. Philip, Magnetic Nanofluids (Ferrofluids): Recent Advances, Applications, Challenges, and Future Directions, *Adv. Colloid Interface Sci.*, 2023, **311**, 102810, DOI: **10.1016/j.cis.2022.102810**.

4 M. T. López-López, A. Gómez-Ramírez, L. Rodríguez-Arco, J. D. G. Durán, L. Iskakova and A. Zubarev, Colloids on the Frontier of Ferrofluids. Rheological Properties, *Langmuir*, 2012, **28**(15), 6232–6245, DOI: **10.1021/la204112w**.

5 V. F. Puntes, D. Zanchet, C. K. Erdonmez and A. P. Alivisatos, Synthesis of Hcp-Co Nanodisks, *J. Am. Chem. Soc.*, 2002, **124**(43), 12874–12880, DOI: **10.1021/ja027262g**.

6 C. P. Gibson and K. J. Putzer, Synthesis and Characterization of Anisometric Cobalt Nanoclusters, *Science*, 1995, **267**(5202), 1338–1340, DOI: **10.1126/science.267.5202.1338**.

7 Y. Yang, M. Li, Y. Wu, T. Wang, E. S. G. Choo, J. Ding, B. Zong, Z. Yang and J. Xue, Nanoscaled Self-Alignment of Fe_3O_4 Nanodiscs in Ultrathin RGO Films with Engineered Conductivity for Electromagnetic Interference Shielding, *Nanoscale*, 2016, **8**(35), 15989–15998, DOI: **10.1039/C6NR04539A**.

8 R. C. Pullar, Hexagonal Ferrites: A Review of the Synthesis, Properties and Applications of Hexaferrite Ceramics, *Prog. Mater. Sci.*, 2012, **57**(7), 1191–1334, DOI: **10.1016/j.pmatsci.2012.04.001**.

9 J. J. Went, G. W. Rathenau, E. W. Gorter and G. W. van Oosterhout, Hexagonal Iron-Oxide Compounds as Permanent-Magnet Materials, *Phys. Rev.*, 1952, **86**(3), 424–425, DOI: **10.1103/PhysRev.86.424.2**.

10 D. Lisjak and M. Drofenik, The Low-Temperature Formation of Barium Hexaferrites, *J. Eur. Ceram. Soc.*, 2006, **26**(16), 3681–3686, DOI: **10.1016/j.jeurceramsoc.2005.12.014**.

11 J. Hu, T. Gorsak, E. Martín Rodríguez, D. Calle, T. Muñoz-Ortiz, D. Jaque, N. Fernández, L. Cussó, F. Rivero, R. Aguilar Torres, J. García Solé, A. Mertelj, D. Makovec, M. Desco, D. Lisjak, F. Alfonso, F. Sanz-Rodríguez and D. H. Ortgies, Magnetic Nanoplatelets for High Contrast Cardiovascular Imaging by Magnetically Modulated Optical Coherence Tomography, *ChemPhotoChem*, 2019, **3**(7), 529–539, DOI: 10.1002/cptc.201900071.

12 T. Goršak, M. Drab, D. Križaj, M. Jeran, J. Genova, S. Kralj, D. Lisjak, V. Kralj-Iglič, A. Iglič and D. Makovec, Magneto-Mechanical Actuation of Barium-Hexaferrite Nanoplatelets for the Disruption of Phospholipid Membranes, *J. Colloid Interface Sci.*, 2020, **579**, 508–519, DOI: 10.1016/j.jcis.2020.06.079.

13 Y. Cheng, M. E. Muroski, D. C. M. C. Petit, R. Mansell, T. Vemulkar, R. A. Morshed, Y. Han, I. V. Balyasnikova, C. M. Horbinski, X. Huang, L. Zhang, R. P. Cowburn and M. S. Lesniak, Rotating Magnetic Field Induced Oscillation of Magnetic Particles for *in Vivo* Mechanical Destruction of Malignant Glioma, *J. Controlled Release*, 2016, **223**, 75–84, DOI: 10.1016/j.jconrel.2015.12.028.

14 M. Shuai, A. Klittnick, Y. Shen, G. P. Smith, M. R. Tuchband, C. Zhu, R. G. Petschek, A. Mertelj, D. Lisjak, M. Čopič, J. E. Maclennan, M. A. Glaser and N. A. Clark, Spontaneous Liquid Crystal and Ferromagnetic Ordering of Colloidal Magnetic Nanoplates, *Nat. Commun.*, 2016, **7**(1), 10394, DOI: 10.1038/ncomms10394.

15 M. Drofenik, M. Kristl, A. Žnidaršič, D. Hanžel and D. Lisjak, Hydrothermal Synthesis of Ba-Hexaferrite Nanoparticles, *J. Am. Ceram. Soc.*, 2007, **90**(7), 2057–2061, DOI: 10.1111/j.1551-2916.2007.01740.x.

16 M. Drofenik, I. Ban, D. Makovec, A. Žnidaršič, Z. Jagličić, D. Hanžel and D. Lisjak, The Hydrothermal Synthesis of Super-Paramagnetic Barium Hexaferrite Particles, *Mater. Chem. Phys.*, 2011, **127**(3), 415–419, DOI: 10.1016/j.matchemphys.2011.02.037.

17 D. Lisjak and M. Drofenik, Chemical Substitution—An Alternative Strategy for Controlling the Particle Size of Barium Ferrite, *Cryst. Growth Des.*, 2012, **12**(11), 5174–5179, DOI: 10.1021/cg301227r.

18 D. Primc, D. Makovec, D. Lisjak and M. Drofenik, Hydrothermal Synthesis of Ultrafine Barium Hexaferrite Nanoparticles and the Preparation of Their Stable Suspensions, *Nanotechnology*, 2009, **20**(31), 315605, DOI: 10.1088/0957-4484/20/31/315605.

19 T. Goršak, D. Makovec, U. Javornik, B. Belec, S. Kralj and D. Lisjak, A Functionalization Strategy for the Dispersion of Permanently Magnetic Barium-Hexaferrite Nanoplatelets in Complex Biological Media, *Colloids Surf., A*, 2019, **573**, 119–127, DOI: 10.1016/j.colsurfa.2019.04.051.

20 P. Hribar Boštjančič, M. Tomšič, A. Jamnik, D. Lisjak and A. Mertelj, Electrostatic Interactions between Barium Hexaferrite Nanoplatelets in Alcohol Suspensions, *J. Phys. Chem. C*, 2019, **123**(37), 23272–23279, DOI: 10.1021/acs.jpcc.9b07455.

21 *Nanoparticles: Synthesis, Stabilization, Passivation, and Functionalization*, ed. R. Nagarajan and T. A. Hatton, ACS Symposium Series, American Chemical Society, Washington, DC, 2008, vol. 996, DOI: 10.1021/bk-2008-0996.

22 M. Barrow, A. Taylor, P. Murray, M. J. Rosseinsky and D. J. Adams, Design Considerations for the Synthesis of Polymer Coated Iron Oxide Nanoparticles for Stem Cell Labelling and Tracking Using MRI, *Chem. Soc. Rev.*, 2015, **44**(19), 6733–6748, DOI: 10.1039/C5CS00331H.

23 H. Heinz, C. Pramanik, O. Heinz, Y. Ding, R. K. Mishra, D. Marchon, R. J. Flatt, I. Estrela-Lopis, J. Llop, S. Moya and R. F. Ziolo, Nanoparticle Decoration with Surfactants: Molecular Interactions, Assembly, and Applications, *Surf. Sci. Rep.*, 2017, **72**(1), 1–58, DOI: 10.1016/j.surfrep.2017.02.001.

24 S. Ovtar, D. Lisjak and M. Drofenik, Preparation of Oriented Barium Hexaferrite Films by Electrophoretic Deposition: Preparation of Oriented Barium Hexaferrite Films, *J. Am. Ceram. Soc.*, 2011, **94**(10), 3373–3379, DOI: 10.1111/j.1551-2916.2011.04500.x.

25 D. Makovec, B. Belec, T. Goršak, D. Lisjak, M. Komelj, G. Dražić and S. Gyergyek, Discrete Evolution of the Crystal Structure during the Growth of Ba-Hexaferrite Nanoplatelets, *Nanoscale*, 2018, **10**(30), 14480–14491, DOI: 10.1039/C8NR03815E.

26 D. Makovec, D. Primc, S. Šturm, A. Kodre, D. Hanžel and M. Drofenik, Structural Properties of Ultrafine Ba-Hexaferrite Nanoparticles, *J. Solid State Chem.*, 2012, **196**, 63–71, DOI: 10.1016/j.jssc.2012.07.043.

27 G. W. Rathenau, E. W. Gorter, G. W. van Oosterhout and J. J. Went, Ferroxdure a Class of New Permanent Magnet Materials, *Phillips Tech. Rev.*, 1952, **13**(7), 194–208.

28 D. Lisjak, S. Ovtar, J. Kovač, L. Gregoratti, B. Aleman, M. Amati, M. Fanetti and D. Makovec, A Surface-Chemistry Study of Barium Ferrite Nanoplates with DBSa-Modified Surfaces, *Appl. Surf. Sci.*, 2014, **305**, 366–374, DOI: 10.1016/j.apsusc.2014.03.092.

29 R. Pattanayak, S. Panigrahi, T. Dash, R. Muduli and D. Behera, Electric Transport Properties Study of Bulk $BaFe_{12}O_{19}$ by Complex Impedance Spectroscopy, *Phys. B*, 2015, **474**, 57–63, DOI: 10.1016/j.physb.2015.06.006.

30 R. Hunter, *Zeta Potential in Colloid Science: Principles and Applications (Colloid Sciences Series)*, Academic Press, 1st edn, 1989.

31 R. C. Wilhoit, J. Chao and K. R. Hall, Thermodynamic Properties of Key Organic Oxygen Compounds in the Carbon Range C_1 to C_4. Part 1. Properties of Condensed Phases, *J. Phys. Chem. Ref. Data*, 1985, **14**(1), 1–175.